The Astrophysical Journal, 881:137 (7pp), 2019 August 20 https://doi.org/10.3847/1538-4357/ab2ed0

Using Spatial Curvature with H II Galaxies and Cosmic Chronometers to Explore the Tension in H_0

Cheng-Zong Ruan[1], Fulvio Melia[2], Yu Chen[1], and Tong-Jie Zhang[1,3]
[1] Department of Astronomy, Beijing Normal University, Beijing 100875, People's Republic of China
[2] Department of Physics, The Applied Math Program, and Department of Astronomy, The University of Arizona, AZ 85721, USA; fmelia@email.arizona.edu
[3] Institute for Astronomical Science, Dezhou University, Dezhou 253023, People's Republic of China
Received 2019 January 19; revised 2019 June 7; accepted 2019 July 1; published 2019 August 21

Abstract

We present a model-independent measurement of spatial curvature Ω_k in the Friedmann–Lemaître–Robertson–Walker universe, based on observations of the Hubble parameter $H(z)$ using cosmic chronometers, and a Gaussian process (GP) reconstruction of the H II galaxy Hubble diagram. We show that the imposition of spatial flatness (i.e., $\Omega_k = 0$) easily distinguishes between the Hubble constant measured with *Planck* and that based on the local distance ladder. We find an optimized curvature parameter $\Omega_k = -0.120^{+0.168}_{-0.147}$ when using the former (i.e., $H_0 = 67.66 \pm 0.42$ km s^{-1} Mpc^{-1}), and $\Omega_k = -0.298^{+0.122}_{-0.088}$ for the latter ($H_0 = 73.24 \pm 1.74$ km s^{-1} Mpc^{-1}). The quoted uncertainties are extracted by Monte Carlo sampling, taking into consideration the covariances between the function and its derivative reconstructed by GP. These data therefore reveal that the condition of spatial flatness favors the *Planck* measurement, while ruling out the locally inferred Hubble constant as a true measure of the large-scale cosmic expansion rate at a confidence level of $\sim 3\sigma$.

Key words: cosmological parameters – distance scale

1. Introduction

One of the fundamental assumptions in modern cosmology is that, on large scales, the universe is described by the homogeneous and isotropic Friedmann–Lemaître–Robertson–Walker (FLRW) metric. The symmetries of this spacetime reduce the 10 independent components of the metric tensor to a single function of time—the scale factor $a(t)$, and a constant—the spatial curvature parameter k, which may take on the values -1 (for an open universe), $+1$ (closed), or 0 (flat). The constant k is often absorbed into the so-called curvature density parameter, $\Omega_k \equiv -kc^2/(a_0H_0)^2$, where c is the speed of light, and $a_0 \equiv a(t_0)$ and the Hubble parameter $H_0 \equiv H(t_0)$ take on their respective values at time t_0 (i.e., today). Thus, the universe is open if $\Omega_k > 0$, spatially flat if $\Omega_k = 0$, and closed if $\Omega_k < 0$. Knowing which of these three possibilities describes the universe is crucial for a complete understanding of its evolution and the nature of dark energy. A significant deviation from zero spatial curvature would have a profound impact on the underlying physics and the inflation paradigm, in part because one of the roles attributed to the inflaton field is that of rapidly expanding the universe to asymptotic flatness, regardless of whether or not it was flat to begin with.

Current cosmological observations strongly favor a flat (or nearly flat) universe, e.g., based on combined *Planck* and baryon acoustic oscillation measurements, that suggest $\Omega_k = 0.0007 \pm 0.0019$ at the 68% confidence level (Planck Collaboration et al. 2018).[4] These constraints, however, are based on the preassumption of a particular cosmological model, such as ΛCDM. Since the curvature parameter is a purely geometric quantity, however, it should be possible to measure or constrain the value of Ω_k from the data using a model-independent method. For a nonexhaustive set of references on this topic, see Bernstein (2006), Knox (2006), Clarkson et al. (2007), Oguri et al. (2012), Li et al. (2014, 2016a, 2016b, 2018), Räsänen et al. (2015), Cai et al. (2016), Yu & Wang (2016), Wei & Wu (2017), Xia et al. (2017), Denissenya et al. (2018), and Wei (2018). A typical curvature measurement methodology is based on the distance sum rule in the FLRW metric using strong lensing (Bernstein 2006; Räsänen et al. 2015), which provides the angular diameter distance between the observer and lens, the observer and source, and the lens and source.

In this paper, we follow a new, model-independent methodology, that combines the observed Hubble parameter $H(z)$ with an independent measurement of the luminosity distance $d_L(z)$ (Clarkson et al. 2007). With this approach, one needs to have a continuous realization of the distance $d_L(z)$ and its derivative $d_L'(z)$ with respect to redshift. A model-independent smoothing technique, based on the use of Gaussian processes (GP), can provide these quantities together with their respective uncertainties and covariances (see, e.g., Seikel et al. 2012; Yennapureddy & Melia 2017). Using GP reconstruction, one can calculate a continuous luminosity distance and its derivative using H II galaxies (H IIGx) and giant extragalactic H II regions (GEHR) as standard candles (Terlevich & Melnick 1981; Chávez et al. 2012, 2014; Terlevich et al. 2015; Wei et al. 2016; and other references cited therein). Then, the luminosity distance $d_L(z)$ may be transformed into the curvature-dependent Hubble parameter $H(z; \Omega_k)$ according to geometric relations derived from the FLRW metric. Finally, by carrying out χ^2 minimization on the observed differences between $H(z)$ and $H(z; \Omega_k)$, one may thereby optimize the value of Ω_k in a model-independent way.

There are several possible applications of this approach that will be explored in subsequent papers. Here, we apply this method to one of the most timely and important problems emerging from the latest cosmological data—the nonignorable

[4] The *Planck* 2018 cosmic microwave background (CMB) temperature and polarization power spectra data singly favor a mildly closed universe, i.e., $\Omega_k = -0.044^{+0.018}_{-0.015}$ (Planck Collaboration et al. 2018). Other studies have found that the *Planck* 2015 CMB anisotropy data also favor a mildly closed universe (Park & Ratra 2018, 2019).

tension between the value of H_0 measured with the local distance ladder (e.g., Riess et al. 2016)—consistently yielding a value $\sim$73 km s^{-1} Mpc^{-1} and an impressively small error of $\sim$2%–3%—and the value measured with *Planck*, based on the fluctuation spectrum of the cosmic microwave background (CMB; Planck Collaboration et al. 2018), i.e., 67.66 ± 0.42 km s^{-1} Mpc^{-1}. These two measurements of H_0 are discrepant at a level exceeding 3σ. Measurements of the spatial curvature parameter Ω_k are often invoked to test inflationary theory, given that a principal role of the inflaton field is to drive the universal expansion to asymptotic flatness. In this paper, we reverse this procedure by instead presuming that the universe is flat and using the $H(z)$ and H II galaxy observations to then examine which of these two values of H_0 is more consistent with this assumption.

We first briefly summarize the methodology of measuring Ω_k using H II galaxies and cosmic chronometers in Section 2. We then describe the relevant data sets in Section 3, and present the results of our analysis in Section 4. We then discuss these results in Section 5, where we conclude that this test strongly favors the *Planck* value as the true representation of the expansion rate on large scales.

2. Methodology

2.1. Luminosity Distance and Distance Modulus

The hydrogen gas ionized by massive star clusters in H II galaxies emits prominent Balmer lines in Hα and Hβ (Terlevich & Melnick 1981; Kunth & Östlin 2000). The luminosity L(Hβ) in Hβ in these systems is strongly correlated with the ionized gas velocity dispersion σ_v of the ionized gas (Terlevich & Melnick 1981), (presumably) because both the intensity of ionizing radiation and σ_v increase with the starburst mass (Siegel et al. 2005). The relatively small scatter in the relationship between L(Hβ) and σ_v allows these galaxies and local H II regions to be used as standard candles (Terlevich et al. 2015; Wei et al. 2016; Yennapureddy & Melia 2017; Leaf & Melia 2018). The emission-line luminosity versus ionized gas velocity dispersion correlation can be approximated as (Chávez et al. 2012)

$$\log\left[\frac{L(\mathrm{H}\beta)}{\mathrm{erg\ s^{-1}}}\right] = \alpha \log\left[\frac{\sigma_v(\mathrm{H}\beta)}{\mathrm{km\ s^{-1}}}\right] + \kappa, \tag{1}$$

where α and κ are constants. With this L–σ_v relation, and the luminosity distance of an H IIGx,

$$d_L = \left[\frac{L(\mathrm{H}\beta)}{4\pi F(\mathrm{H}\beta)}\right]^{1/2}, \tag{2}$$

we write

$$\log\left(\frac{d_L}{\mathrm{Mpc}}\right) = 0.5\left[\alpha \log\left(\frac{\sigma_v(\mathrm{H}\beta)}{\mathrm{km\ s^{-1}}}\right) - \log\left(\frac{F(\mathrm{H}\beta)}{\mathrm{erg\ s^{-1}\ cm^{-2}}}\right)\right] + 0.5\kappa - 25.04, \tag{3}$$

where F (Hβ) is the reddening corrected Hβ flux.

Note that the luminosity distance $d_L \equiv \sqrt{L/(4\pi F)}$ is conventionally defined by the bolometric luminosity and flux, whereas here we approximate this relation with the luminosity L (Hβ) and flux F(Hβ) pertaining to the Hβ line. When selecting H II galaxies from spectroscopic surveys, the most import criteria are (i) the identification of the largest equivalent width (EW) in the galaxies' emission lines, with EW (Hβ) > 50 Å or EW (H α) > 200 Å in their rest frame, and (ii) that the emission regions are extremely compact. The lower limits guarantee that the selected H IIGx are comprised of systems in which the luminosity is dominated by single and very young starbursts (less than 5 Myr in age; Terlevich et al. 2015). The bolometric flux of the H IIGx may thereby be regarded as constituting principally the Hβ line.

The two "nuisance" parameters α and κ (or its Hubble-free replacement, δ; see definition below) in principle need to be optimized simultaneously with those of the cosmological model. Wei et al. (2016) have found, however, that their values deviate by at most only a tiny fraction of their 1σ errors, regardless of which model is adopted. This is the important step that allows us to use the H II galaxy Hubble diagram in a model-independent way. For example, these authors found that $\alpha = 4.86^{+0.08}_{-0.07}$ and $\delta = 32.38^{+0.29}_{-0.29}$ in the $R_h = ct$ cosmology (Melia & Shevchuk 2012), while $\alpha = 4.89^{+0.09}_{-0.09}$ and $\delta = 32.49^{+0.35}_{-0.35}$ in ΛCDM. Such small differences fall well within the observational uncertainty and, following Melia (2018b), we therefore simply adopt a reasonable representation of the average value for these parameters, i.e., $\alpha = 4.87^{+0.11}_{-0.08}$ and $\delta = 32.42^{+0.42}_{-0.33}$. We emphasize, however, that this relative model-independence of α and δ is based on the best-fit analysis using $R_h = ct$ and various versions of ΛCDM (Wei et al. 2016). The caveat here is that if one chooses an even more exotic model that differs from ΛCDM and $R_h = ct$ by greater amounts, these parameters may themselves vary more strongly than we assume here.

The Hubble-free parameter δ is defined as follows:

$$\delta \equiv -2.5\kappa - 5\log\left(\frac{H_0}{\mathrm{km\ s^{-1}\ Mpc^{-1}}}\right) + 125.2, \tag{4}$$

with which one may express the dimensionless luminosity distance $(H_0\ d_L)/c$ as

$$\left(\frac{H_0}{c}\right) d_L(z) = \frac{10^{\eta(z)/5}}{c/(\mathrm{km\ s^{-1}})}, \tag{5}$$

where

$$\eta = -\delta + 2.5\left(\alpha \log\left[\frac{\sigma_v(\mathrm{H}\beta)}{\mathrm{km\ s^{-1}}}\right] - \log\left[\frac{F(\mathrm{H}\beta)}{\mathrm{erg\ s^{-1}\ cm^{-2}}}\right]\right), \tag{6}$$

and the speed of light c is 299792.458 km s^{-1}. Equation (6) is an approximation for the distance modulus μ under the assumption of the L–σ_v relation in Equation (1). In addition, $\eta(z)$ defined in Equation (5) differs by a constant from

$$\mu \equiv 5\log\left(\frac{d_L}{\mathrm{Mpc}}\right) + 25, \tag{7}$$

such that

$$\mu - \eta = -5\log\left(\frac{H_0}{\mathrm{km\ s^{-1}\ Mpc^{-1}}}\right) + 25.2. \tag{8}$$

Given the flux and gas velocity dispersion (along with their uncertainties) of H IIGx and GEHR, one can get the "shifted" distance modulus $\eta(z)$ using Equation (6). And for each measurement of $H(z_j)$ using cosmic chronometers at redshift z_j,

we use a model-independent GP reconstruction to get the corresponding $\eta(z_j)$ and $\eta'(z_j)$ as well as their uncertainties and covariances, where the derivative is defined by

$$\eta' \equiv \frac{d\eta}{d\log_{10} z}. \tag{9}$$

The systematic uncertainties of the H II-galaxy probe, based on the $L(\mathrm{H}\beta)-\sigma$ correlation, still need to be better understood. These consist of the size of the starburst, the age of the burst, the oxygen abundance of H II galaxies and the internal extinction correction (Chávez et al. 2016). The scatter found in this $L(\mathrm{H}\beta)-\sigma$ relation indicates that it probably depends on a second parameter. Some progress has been made to mitigate these uncertainties. For example, Chávez et al. (2016) found that, for samples of local H II galaxies, the size of the star-forming region can be used as this second parameter. Another important consideration is the exclusion of systems supported by rotation, which obviously distorts the $L(\mathrm{H}\beta)-\sigma$ relationship. Melnick et al. (1988) and Chávez et al. (2016) suggested using an upper limit of the velocity dispersion $\log[\sigma(\mathrm{H}\beta)/\mathrm{km\ s^{-1}}] \sim 1.8$ to minimize this possibility, although the catalog of suitable sources is then greatly reduced. However, even with this limitation, there is no guarantee that this systematic effect is completely eliminated.

2.2. Geometric Relation in the FLRW Universe

In the FLRW metric, the radial comoving distance $d_c(z)$ of a galaxy at redshift z is expressed as

$$d_c(z) = c\int_0^z \frac{dz'}{H(z')}. \tag{10}$$

The relation between comoving and luminosity distances changes as the sign of Ω_k changes:

$$\frac{d_L(z)}{1+z} = \begin{cases} \frac{c}{H_0}\frac{1}{\sqrt{\Omega_k}}\sinh\left[\sqrt{\Omega_k}\frac{H_0}{c}d_c(z)\right] & \text{for } \Omega_k > 0 \\ d_c(z) & \text{for } \Omega_k = 0. \\ \frac{c}{H_0}\frac{1}{\sqrt{|\Omega_k|}}\sin\left[\sqrt{|\Omega_k|}\frac{H_0}{c}d_c(z)\right] & \text{for } \Omega_k < 0 \end{cases} \tag{11}$$

To find a relation between the H IIGx and $H(z)$ data, we note that the derivative of Equation (10) simply gives $d_c'(z) \equiv d/dz(d_c[z]) = c/H(z)$. This suggests a similarly useful operation with Equation (11), from which a new relation between $H(z)$ and the luminosity distance may be extracted:

$$E(z) \equiv \frac{H(z)}{H_0} = \begin{cases} \frac{c}{H_0 f(z)}\sqrt{1+\left[\frac{H_0 d_L(z)}{c}\frac{\sqrt{\Omega_k}}{1+z}\right]^2} & \Omega_k > 0 \\ c/[H_0 f(z)] & \Omega_k = 0, \\ \frac{c}{H_0 f(z)}\sqrt{1-\left[\frac{H_0 d_L(z)}{c}\frac{\sqrt{|\Omega_k|}}{1+z}\right]^2} & \Omega_k < 0 \end{cases} \tag{12}$$

and

$$f(z) \equiv \frac{d}{dz}\left[\frac{d_L(z)}{1+z}\right] = \frac{d_L'(z)}{1+z} - \frac{d_L(z)}{(1+z)^2}. \tag{13}$$

Equation (12) relates the luminosity distance $d_L(z)$ to the Hubble expansion rate $H(z)$ in the FLRW universe, in which the former may be extracted with GP reconstruction of the H IIGx Hubble diagram, while the latter may be found using cosmic chronometers. We employ two distinct values of the Hubble constant to turn the Hubble parameter $H(z)$ into a dimensionless quantity. These are the *Planck* value and that measured locally using the distance ladder:

$$\textit{Planck}\ \text{value:}\quad H_0 = 67.66 \pm 0.42\ \mathrm{km\ s^{-1}\ Mpc^{-1}}, \tag{14}$$

$$\text{local value:}\quad H_0 = 73.24 \pm 1.74\ \mathrm{km\ s^{-1}\ Mpc^{-1}}. \tag{15}$$

For each of these quantities, we extract a purely geometric measurement of the curvature parameter Ω_k though, as noted earlier, our intention is clearly to probe which of these two disparate values of H_0 is more consistent with spatial flatness.

For consistency with the GP results, we represent the dimensionless luminosity distance $(H_0\, d_L)/c$ using the (shifted) distance modulus η (Equation (6)). The dimensionless Hubble parameter is

$$E(z;\,\Omega_k) = \begin{cases} g(z)\sqrt{1+\left[\frac{\sqrt{\Omega_k}\ 10^{\eta(z)/5}}{[c/(\mathrm{km\ s^{-1}})](1+z)}\right]^2} & \Omega_k > 0 \\ g(z) & \Omega_k = 0, \\ g(z)\sqrt{1-\left[\frac{\sqrt{|\Omega_k|}\ 10^{\eta(z)/5}}{[c/(\mathrm{km\ s^{-1}})](1+z)}\right]^2} & \Omega_k < 0 \end{cases} \tag{16}$$

where

$$g(z) = \left[\frac{1}{5z(1+z)}\frac{10^{\eta(z)/5}\,\eta'(z)}{c/(\mathrm{km\ s^{-1}})} - \frac{1}{(1+z)^2}\frac{10^{\eta(z)/5}}{c/(\mathrm{km\ s^{-1}})}\right]^{-1} \tag{17}$$

2.3. Uncertainty of $E(z;\,\Omega_k)$

The covariance between η and η' may be found with GP reconstruction, i.e., $\mathrm{Cov}(\eta[z],\,\eta'[z]) \neq 0$. In the context of GP, the values $\eta_\star \equiv \eta(z_\star)$ and $\eta'_\star \equiv \eta'(z_\star)$ at any redshift point $z_\star$ follow a multivariate Gaussian distribution (Seikel et al. 2012)

$$\begin{pmatrix}\eta_\star \\ \eta'_\star\end{pmatrix} \sim \mathcal{N}\left[\begin{pmatrix}\bar{\eta}_\star \\ \bar{\eta}'_\star\end{pmatrix}, \begin{pmatrix}\mathrm{Var}(\eta_\star) & \mathrm{Cov}(\eta_\star,\,\eta'_\star) \\ \mathrm{Cov}(\eta_\star,\,\eta'_\star) & \mathrm{Var}(\eta'_\star)\end{pmatrix}\right], \tag{18}$$

where $\bar{\eta}$, $\bar{\eta}'$, $\mathrm{Cov}(\eta,\,\eta')$, and $\mathrm{Var}(\eta,\,\eta')$ are computed with the GP code called GaPP[5] developed by Seikel et al. (2012).

For every redshift point z_i at which a measurement of $H(z_i)$ is made, the uncertainty $\sigma_{E_i(\Omega_k)}$ is determined by Monte Carlo sampling, where $\begin{pmatrix}\eta_i \\ \eta'_i\end{pmatrix}$ is extracted from the probability distribution given by Equation (18). For example, we generate $N_{\mathrm{MC}} = 10^4$ points,

$$\{\eta_i^{(j)},\,\eta_i'^{(j)}\}_{j=1}^{N_{\mathrm{MC}}} \quad\Rightarrow\quad \{E_i(\eta_i^{(j)},\,\eta_i'^{(j)})\}_{j=1}^{N_{\mathrm{MC}}}, \tag{19}$$

and from these calculate the standard deviation σ_{E_i} of this array.

3. Data

3.1. Hubble Parameter from Cosmic Chronometers

The Hubble parameter, $H(z) \equiv \dot{a}/a$, is the expansion rate of the FLRW universe in terms of the scale factor $a(t)$ and its time derivative $\dot{a} \equiv da/dt$. The Hubble expansion rate may be deduced in a model-independent fashion from cosmic chronometers, using the differential ages of galaxies, as proposed by

[5] http://www.acgc.uct.ac.za/~seikel/GAPP/main.html

Table 1
Hubble Parameter $H(z)$ from Cosmic Chronometers

z	$H(z)$ (km s^{-1} Mpc^{-1})	References
0.09	69 ± 12	Jimenez et al. (2003)
0.17	83 ± 8	Simon et al. (2005)
0.27	77 ± 14	
0.4	95 ± 17	
0.9	117 ± 23	
1.3	168 ± 17	
1.43	177 ± 18	
1.53	140 ± 14	
1.75	202 ± 40	
0.48	97 ± 62	Stern et al. (2010)
0.88	90 ± 40	
0.1791	75 ± 4	Moresco et al. (2012)
0.1993	75 ± 5	
0.3519	83 ± 14	
0.5929	104 ± 13	
0.6797	92 ± 8	
0.7812	105 ± 12	
0.8754	125 ± 17	
1.037	154 ± 20	
0.07	69 ± 19.6	Zhang et al. (2014)
0.12	68.6 ± 26.2	
0.2	72.9 ± 29.6	
0.28	88.8 ± 36.6	
1.363	160 ± 33.6	Moresco (2015)
1.965	186.5 ± 50.4	
0.3802	83 ± 13.5	Moresco et al. (2016)
0.4004	77 ± 10.2	
0.4247	87.1 ± 11.2	
0.4497	92.8 ± 12.9	
0.4783	80.9 ± 9	

Jimenez & Loeb (2002). We use a sample of 30 $H(z)$ measurements in the redshift range of $0.07 < z < 2.0$, compiled by Moresco et al. (2016), which we list in Table 1. The corresponding dimensionless values in this sample are plotted in Figure 1, using the two distinct values of H_0 shown in Equations (14) and (15).

3.2. Luminosity Distance from GP Reconstruction of the H II Galaxy Hubble Diagram

For the H IIGx Hubble diagram, we extract the 25 high-z H IIGx, 24 GEHRs, and 10 local H IIGx (with $z > 0.07$) from the catalog compiled by Wei et al. (2016), from the observational works of Hoyos et al. (2005), Erb et al. (2006), Chávez et al. (2014), Maseda et al. (2014), Masters et al. (2014), and Terlevich et al. (2015). We exclude other local H IIGx in this catalog because most of them (i.e., 97/107) have a redshift that is less than the minimum redshift ($z_{\rm min} = 0.07$) sampled in the cosmic-chronometer data. The GP reconstructed "shifted" distance modulus, $\eta\{z, \sigma_\eta(z), \eta'(z), \sigma_{\eta'}(z), {\rm Cov}[\eta(z), \eta'(z)]\}$, is calculated from these data, following the prescription described in Yennapureddy & Melia (2017). The distance modulus data and GP reconstruction are shown together in Figure 2. As one may see in this figure, the error of the reconstructed $\eta(z)$ function is smaller than that of the original H IIGx data. The error calculated by the GP reconstruction

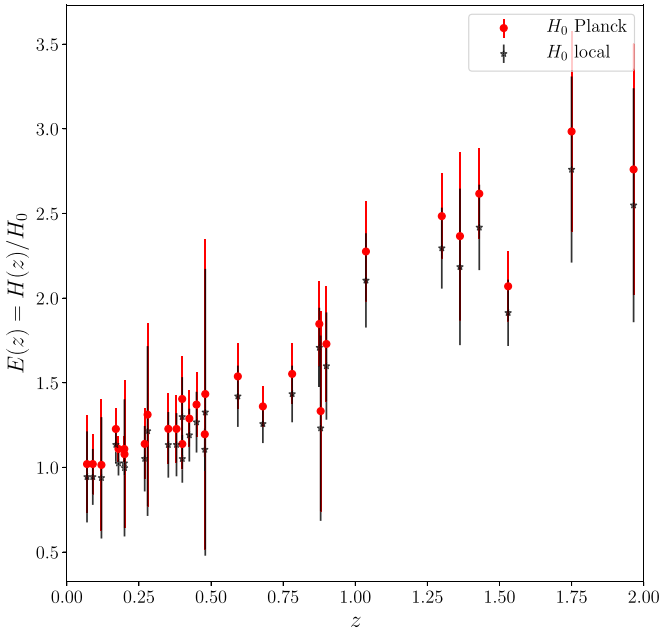

Figure 1. Dimensionless Hubble parameter $E(z) \equiv H(z)/H_0$ data, using two distinct values of the Hubble constant H_0, one from *Planck* (red circle) and the other from the local distance ladder (black star), provided in Equations (14) and (15). The uncertainties in $E(z)$ are due to the uncertainties of both $H(z)$ and H_0, which are estimated by a Monte Carlo method. All of these data are based on observations of cosmic chronometers, listed in Table 1.

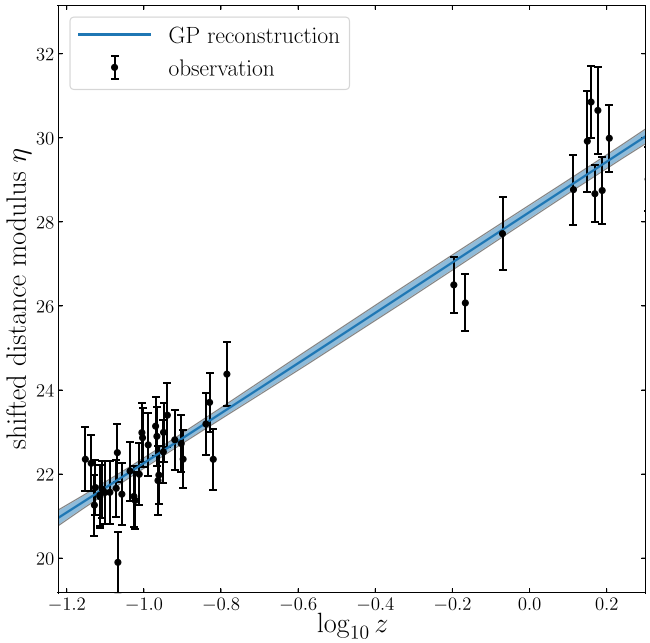

Figure 2. (Shifted) Distance modulus of the currently available HIIGx observations, shown with 1σ error bars, spanning a redshift range of $0.07 \lesssim z \lesssim 2.33$. The GP reconstructed (shifted) distance modulus $\eta(z)$ is shown as a solid blue curve, with its 1σ confidence region (the swath with a lighter shade of blue). The sample consists of 25 high-z HIIGx, 24 giant extragalactic HII regions, and 10 local HIIGx with $z > 0.07$ (Wei et al. 2016; see also Terlevich et al. 2015).

depends on the errors of observational data $\sigma_{\eta_{\rm obs}}$, on the optimized hyperparameter(s) of the GP method, such as the characteristic "bumpiness" parameter σ_f, and on the product of the covariance matrixes $K_* K^{-1} K_*^T$ between the estimation point z_* and data set points $\{ z_i \}$ (see Seikel et al. 2012;

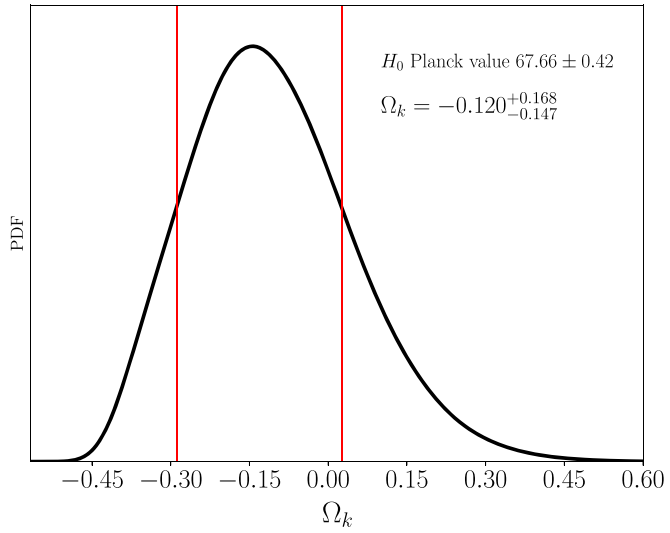

Figure 3. Posterior probability density function of the parameter Ω_k, for the Hubble constant measured by *Planck*, i.e., $H_0 = 67.66 \pm 0.42$ km s^{-1} Mpc^{-1}, showing also the optimized value and its 1σ error.

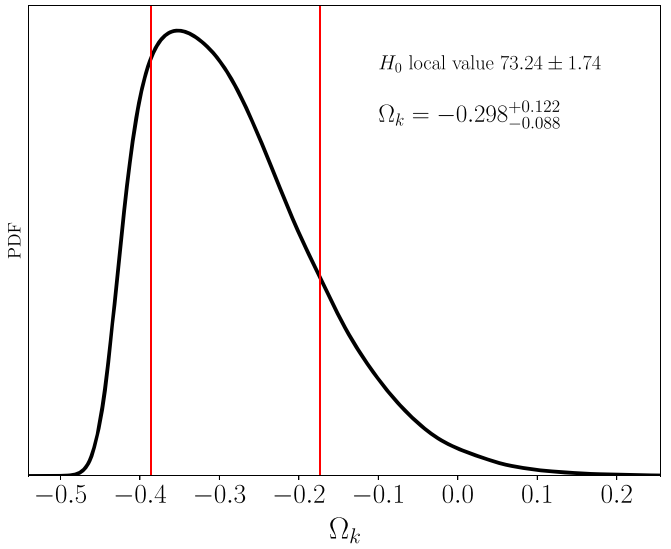

Figure 4. Same as Figure 3, but for the Hubble constant measured with the local distance ladder, i.e., $H_0 = 73.24 \pm 1.74$ km s^{-1} Mpc^{-1}, showing also the optimized value and its 1σ error.

Yennapureddy & Melia 2017). The reconstruction uncertainty $\sigma_{\eta_{\rm GP}}(z_*)$ at z_* will be smaller than $\sigma_{\eta_{\rm obs}}$ when there is a large correlation between the data for the point z_*: $K_* K^{-1} K_*^T > \sigma_f$, which is the most common case with the H II-galaxy data used in this study. Thus the estimated confidence region is smaller than that of the observational data.

4. Results and Discussion

An optimized value of Ω_k may be extracted in a model-independent fashion from fitting the 30 $E^{\rm cc}\{z_i, \sigma_{E^{\rm cc},i}\}$ cosmic-chronometer and $E\{z_i, \sigma_{E,i}\}$ GP reconstructed values of the dimensionless Hubble constant. We use Bayesian statistical methods and the Markov Chain Monte Carlo technique to calculate the posterior probability density function (PDF) of Ω_k, given as

$$p(\Omega_k|\text{data}) \propto \mathcal{L}(\Omega_k, \text{data}) \times p_{\rm prior}(\Omega_k), \tag{20}$$

where

1. $\mathcal{L}(\Omega_k, \text{data}) \propto \exp(-\chi^2/2)$ is the likelihood function, and

$$\chi^2(\Omega_k) = \sum_{i=1}^{N=30} \left\{ \frac{[E_i^{\rm cc} - E_i(\Omega_k)]^2}{\sigma^2_{E^{\rm cc},i} + \sigma^2_{E^{\rm L},i}(\Omega_k)} \right\} \tag{21}$$

   is the chi-squared function;
2. $p_{\rm prior}(\Omega_k)$ is the prior of Ω_k and (assumed) uniform distribution between -1 and 1.

We use the Python module emcee[6] (Foreman-Mackey et al. 2013) to sample from the posterior distribution of Ω_k, and find that its optimized value and 1σ error are

$$\Omega_k = -0.120^{+0.168}_{-0.147} \quad (H_0 \text{ Planck value}), \tag{22}$$

$$\Omega_k = -0.298^{+0.122}_{-0.088} \quad (H_0 \text{ local distance} - \text{ladder value}), \tag{23}$$

for the two distinct values of H_0. The two corresponding PDF plots are shown in Figures 3 and 4, respectively.

We see that the *Planck* measured value of H_0 (Figure 3) is consistent with spatial flatness to within 1σ. This is quite meaningful in the sense that the *Planck* optimization procedure is based on the analysis of anisotropies in the CMB, thought to have originated as quantum fluctuations in the inflaton field. Self-consistency would demand that the value of Ω_k calculated with the *Planck* Hubble constant should therefore support a spatially flat universe—an unavoidable consequence of the inflationary paradigm.

In contrast, we also see that the Hubble constant measured with the local distance ladder (Figure 4) is in significant tension with the requirements of a flat universe. Our results show that Ω_k measured in this way rules out spatial flatness at roughly 3σ. Thus, if this locally measured Hubble constant is a true reflection of the large-scale cosmic expansion rate, our results could be taken as some evidence against inflation as the true solution to the horizon problem (see, e.g., Melia 2013, 2018a).

The disparity between the two distinct values of H_0 may in fact be real, signaling the role of local physics in changing the nearby expansion rate compared to what we see on the largest cosmic scales. Some authors have speculated on the possibility that a local "Hubble bubble" (Shi 1997; Keenan et al. 2013; Romano & Andrés Vallejo 2015; Chiang et al. 2017; Romano 2018) might be influencing the local dynamics within a distance $\sim$300 Mpc (i.e., $z \lesssim 0.07$). If true, such a fluctuation might lead to anomalous velocities within this region, causing the nearby expansion to deviate somewhat from a pure Hubble flow. This effect could be the reason we are seeing nearby velocities slightly larger than Hubble, implying larger than expected luminosity distances at redshifts smaller than $\sim$0.07. Our findings would be fully consistent with this scenario, given that the data we have used in this paper pertain to sources at redshifts well outside the so-called Hubble bubble. We would therefore expect our analysis to support the *Planck* value of H_0, rather than the locally measured one.

To further validate our results, we have also optimized the value of Ω_k corresponding to an H_0 with a flat probability distribution instead of Gaussian. Considering that the typical

[6] http://dfm.io/emcee/current/

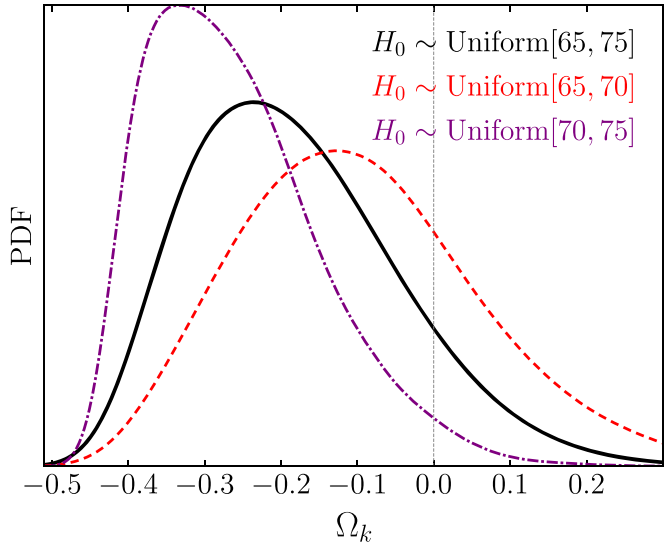

Figure 5. Same as Figure 3, except for a Hubble constant with a uniform distribution in the intervals [65, 75], [65, 70], and [70, 75] km s^{-1} Mpc^{-1}, respectively.

H_0 *Planck* and local distance-ladder values are approximately 67 and 73 km s^{-1} Mpc^{-1}, respectively, we have chosen uniform distributions over three intervals: [65, 75], [65, 70], and [70, 75] (hereafter all values of H_0 are presented in terms of km s^{-1} Mpc^{-1} for conciseness). Following the same data handling pipeline as before, we find that the optimized values and their 1σ errors are

$$\Omega_k = -0.199^{+0.157}_{-0.126},\ H_0 \sim \mathrm{U}[65, 75], \tag{24}$$

$$\Omega_k = -0.110^{+0.171}_{-0.151},\ H_0 \sim \mathrm{U}[65, 70], \tag{25}$$

$$\Omega_k = -0.279^{+0.129}_{-0.098},\ H_0 \sim \mathrm{U}[70, 75], \tag{26}$$

respectively. The corresponding posterior probability distributions are shown in Figure 5.

These curvature constraints validate our conclusion regarding the consistency of H_0 with spatial flatness. The lower H_0 value uniformly distributed between 65 and 70 is in accordance with $\Omega_k = 0$ to within 1σ, while the larger one is not. Therefore, noninformative distributions of H_0 have little impact on our curvature fitting results.

5. Summary

In this paper, we have presented a novel approach to the measurement of the spatial flatness parameter, proportional to Ω_k, which avoids possible biases introduced with the preadoption of a particular cosmological model. Our first application of this method, reported here, has already yielded a significant result, supporting arguments in favor of the *Planck* optimized value of the Hubble constant as being a fair representation of the large-scale cosmic expansion rate. Indeed, the locally measured value of H_0 has been ruled out as a true measure of the "average" Hubble constant at a confidence level of $\sim 3\sigma$.

In this view, our results might also be taken as some evidence in support of the "Hubble bubble" concept, which suggests that locally measured expansion velocities somewhat exceed the Hubble flow due to a below average density, thereby implying larger than normal luminosity distances. Quite tellingly, the data we have used are restricted to redshifts $z \gtrsim 0.07$, which also happens to be near the bubble's termination radius. At the very least, all of these inferences are consistent with each other. A stronger case for these conclusions could be made with measurements of the Hubble parameter at redshifts $z \lesssim 0.07$. We shall initiate this investigation in the near future and report the results elsewhere.

We are grateful to the anonymous referee for several suggestions that have led to an improvement in the presentation of our results. This work was supported by National Key R&D Program of China (2017YFA0402600), the National Science Foundation of China (grant Nos. 11573006 and 11528306), the Fundamental Research Funds for the Central Universities, and the Special Program for Applied Research on Super Computation of the NSFC-Guangdong Joint Fund (the second phase).

ORCID iDs

Cheng-Zong Ruan https://orcid.org/0000-0001-7255-0536
Fulvio Melia https://orcid.org/0000-0002-8014-0593
Tong-Jie Zhang https://orcid.org/0000-0002-1596-529X

References

Bernstein, G. 2006, ApJ, 637, 598
Cai, R.-G., Guo, Z.-K., & Yang, T. 2016, PhRvD, 93, 043517
Chávez, R., Plionis, M., Basilakos, S., et al. 2016, MNRAS, 462, 2431
Chávez, R., Terlevich, E., Terlevich, R., et al. 2012, MNRAS, 425, L56
Chávez, R., Terlevich, R., Terlevich, E., et al. 2014, MNRAS, 442, 3565
Chiang, H. W., Enea Romano, A., Nugier, F., & Chen, P. 2017, arXiv:1706.09734
Clarkson, C., Cortês, M., & Bassett, B. 2007, JCAP, 8, 011
Denissenya, M., Linder, E. V., & Shafieloo, A. 2018, JCAP, 3, 041
Erb, D. K., Steidel, C. C., Shapley, A. E., et al. 2006, ApJ, 646, 107
Foreman-Mackey, D., Hogg, D. W., Lang, D., & Goodman, J. 2013, PASP, 125, 306
Hoyos, C., Koo, D. C., Phillips, A. C., Willmer, C. N. A., & Guhathakurta, P. 2005, ApJL, 635, L21
Jimenez, R., & Loeb, A. 2002, ApJ, 573, 37
Jimenez, R., Verde, L., Treu, T., & Stern, D. 2003, ApJ, 593, 622
Keenan, R. C., Barger, A. J., & Cowie, L. L. 2013, ApJ, 775, 62
Knox, L. 2006, PhRvD, 73, 023503
Kunth, D., & Östlin, G. 2000, A&ARv, 10, 1
Leaf, K., & Melia, F. 2018, MNRAS, 474, 4507
Li, Y.-L., Li, S.-Y., Zhang, T.-J., & Li, T.-P. 2014, ApJL, 789, L15
Li, Z., Ding, X., Wang, G.-J., Liao, K., & Zhu, Z.-H. 2018, ApJ, 854, 146
Li, Z., Gonzalez, J. E., Yu, H., Zhu, Z.-H., & Alcaniz, J. S. 2016a, PhRvD, 93, 043014
Li, Z., Wang, G.-J., Liao, K., & Zhu, Z.-H. 2016b, ApJ, 833, 240
Maseda, M. V., van der Wel, A., Rix, H.-W., et al. 2014, ApJ, 791, 17
Masters, D., McCarthy, P., Siana, B., et al. 2014, ApJ, 785, 153
Melia, F. 2013, A&A, 553, A76
Melia, F. 2018a, EPJC, 78, 739
Melia, F. 2018b, MNRAS, 481, 4855
Melia, F., & Shevchuk, A. S. H. 2012, MNRAS, 419, 2579
Melnick, J., Terlevich, R., & Moles, M. 1988, MNRAS, 235, 297
Moresco, M. 2015, MNRAS, 450, L16
Moresco, M., Pozzetti, L., Cimatti, A., et al. 2016, JCAP, 5, 014
Moresco, M., Verde, L., Pozzetti, L., Jimenez, R., & Cimatti, A. 2012, JCAP, 7, 053
Oguri, M., Inada, N., Strauss, M. A., et al. 2012, AJ, 143, 120
Park, C.-G., & Ratra, B. 2018, arXiv:1801.00213
Park, C.-G., & Ratra, B. 2019, Ap&SS, 364, 82
Planck Collaboration, Aghanim, N., Akrami, Y., et al. 2018, arXiv:1807.06209
Räsänen, S., Bolejko, K., & Finoguenov, A. 2015, PhRvL, 115, 101301
Riess, A. G., Macri, L. M., Hoffmann, S. L., et al. 2016, ApJ, 826, 56
Romano, A. E. 2018, IJMPD, D27, 1850102
Romano, A. E., & Andrés Vallejo, S. 2015, EL, 109, 39002
Seikel, M., Clarkson, C., & Smith, M. 2012, JCAP, 6, 036
Shi, X. 1997, ApJ, 486, 32

Siegel, E. R., Guzmán, R., Gallego, J. P., Orduña López, M., & Rodríguez Hidalgo, P. 2005, MNRAS, 356, 1117
Simon, J., Verde, L., & Jimenez, R. 2005, PhRvD, 71, 123001
Stern, D., Jimenez, R., Verde, L., Kamionkowski, M., & Stanford, S. A. 2010, JCAP, 2, 008
Terlevich, R., & Melnick, J. 1981, MNRAS, 195, 839
Terlevich, R., Terlevich, E., Melnick, J., et al. 2015, MNRAS, 451, 3001
Wei, J.-J. 2018, ApJ, 868, 29
Wei, J.-J., & Wu, X.-F. 2017, ApJ, 838, 160
Wei, J.-J., Wu, X.-F., & Melia, F. 2016, MNRAS, 463, 1144
Xia, J.-Q., Yu, H., Wang, G.-J., et al. 2017, ApJ, 834, 75
Yennapureddy, M. K., & Melia, F. 2017, JCAP, 2017, 029
Yu, H., & Wang, F. Y. 2016, ApJ, 828, 85
Zhang, C., Zhang, H., Yuan, S., et al. 2014, RAA, 14, 1221